Case Studies in Thermal Engineering 26 (2021) 100962

Contents lists available at ScienceDirect

Case Studies in Thermal Engineering

journal homepage: http://www.elsevier.com/locate/csite

Combined magnetic and porosity effects on flow of time-dependent tangent hyperbolic fluid with nanoparticles and motile gyrotactic microorganism past a wedge with second-order slip

Shafiq Hussain [a], Farooq Ahmad [b,f,*], Hela Ayed [b], Muhammad Y Malik [c], Hassan Waqas [e], M. Mossa Al-Sawalha [b], Sajjad Hussain [d,f]

[a] Department of Computer Science, University of Sahiwal, Sahiwal, Pakistan
[b] Department of Mathematics, Colleg of Science, University of Ha'il, Ha'il, Saudi Arabia
[c] Department of Mathematics, Colleg of Science, KK University, Saudi Arabia
[d] Department of Mathematics, Govt. Post Graduate Colleg, Layyah, BZ Uni, Pakistan
[e] Department of Mathematics, Govt. College University, Faisalabad, Pakistan
[f] School of Mechanical and Aero Space Engineering, Nanyang Technological University, Singapore

ARTICLE INFO

Keywords:
Tangent hyperbolic fluids
Nano fluids
Heat and mass transfer
Bioconvection
Motile microorganism
Non-linear thermal radiation
Bvp4c numerical technique

ABSTRACT

This research explores the time-dependent heat transport phenomena for the MHD flow of nanofluids containing motile microorganisms via porous matrix. The fluid flows through a porous stretched wedge with second-order slip and Nield boundary. Different physical and geometric parameters are included to achieve more practicable effects. The developed equations are converted into a non - dimensional form through the use of appropriate similarity functions. The mathematical formulation is built for these transmuted equations using the built-in Matlab software bvp4c. Differences in physical quantities namely skin friction coefficient $-f''(0)$, local Nusselt number $-\theta'(0)$, Sherwood number $\varphi'(0)$and microorganism organism density $-\chi'(0)$ have also been identified under the influences of emerging parameters. Bioconvection caused by microorganisms stabilized nanomaterials, resulting in effective thermal delivery. The findings showed good consistency as compared to the current literature. The higher mixed convection parameter contributes to the quantities of flow viscosity, temperature, and nanoparticle concentration in boundary conditions. The incremented slip parameter γ precedes the flow speed. The skin friction factor $-f''(0)$ reduces against unsteadiness parameter A, Hartree pressure gradient β, velocity ratio parameterλ, bouancy ratio parameterNr but it develops progressively when the parameters M, We, n, λ and bioconvection Rayleigh number Nc are incremented. The elaborated discussion is also presented with graphical and tabular illustrations.

* Corresponding author. Department of Mathematics, Colleg of Science, University of Ha'il, Ha'il, Saudi Arabia.
E-mail addresses: drshafiq@uosahiwal.edu.pk (S. Hussain), ahmad.farooq@uoh.edu.sa, ahmad.farooq@ntu.edu.sg (F. Ahmad), h.ayed@uoh.edu.sa (H. Ayed), drmymalk@kku.edu.sa (M.Y. Malik), syedhasanwaqas@hotmail.com (H. Waqas), m.alswalha@uoh.edu.sa (M.M. Al-Sawalha), hussain.sajjad@gpgcl.giccl.edu.pk, sajjadgut@gmail.com (S. Hussain).

https://doi.org/10.1016/j.csite.2021.100962
Received 28 February 2021; Received in revised form 20 March 2021; Accepted 21 March 2021
Available online 30 March 2021

1. Introduction

Non-Newtonian fluids are significant due to their environmental impact and many applications in nuclear material slurries, solvents, bio-fluids in tumor materials, extrusion of polymer matrix fluids, emulsions, and polyethylene. Shear-thinning, thermal conductivity and viscoelasticity are among some of the extraordinary characteristics of non-Newtonian fluids that have several perspectives [1,2]. Various rheological models are implemented to establish the non-Newtonian behavior of fluids. Consequently, the related studies demonstrate improvements in momentum conservation equations. The composition is based on the distinctive rheological properties of these non-Newtonian fluids and has been used to represent these fluids. Reynolds stress models, Sisko model, Williamson model, power-law model, the differential Reiner-Rivlin model, and the Carreau model are instances of some of the mostly used models. Various studies [3–5] are proposed to establish the flow and heat transfer of real fluids. Akbar et al. [6] persuaded MHD convective heat transfer results for tangent hyperbolic fluid via the stretched wall. Ali et al. [7] obtained generalized findings on thermal radiation and heat generation/absorption in nanofluid flow regime. Khan et al. [8] explored 3-D axisymmetric Carreau nanofluid flow near the Homann stagnation region along with chemical reaction and Fourier's and Fick's laws. Nasser et al. [9] investigated the boundary condition movement of tangential hyperbolic fluid through the vertical stretched cylinder. Salahuddin et al. [10] investigated the influence of the gravity force and variable heat capacity on the convection of the hyperbolic tangent fluid via the stretching cylinder.

Intensification of heat transfer rates are important for the smooth operation and maintenance of a multitude of conditions in the engineering and manufacturing sectors. Various practices have arisen, including airing, coolants, and various other forms of heat exchangers, to deal with the phenomena of convection. Consequently, enhancing the thermal conductivity of fluids has been an attractive field for the scientific community. For scientists, biotechnology has had a significant influence on recent developments. Nanofluid, developed by Choi [11] in 1995, received a great deal of emminence. Nanofluids are known as being the most important coolants in mechanical and software development. There is a mixture of microscopic particles dissolved in the base fluid that boosts the thermal conductivity of nanomaterials interactions. Many other attempts have been made to investigate the anomaly with nanomaterials. For example, Buongiorno [12] has researched two essential slip processes, including thermophoresis and Brownian features, to look up the rate of heat transport. The flow of nanofluid through stretching surfaces that use the Buongiorno model is proposed by Khan and Pop [13]. Bhatti et al. [14] investigated the thermal diffusion and Brownian motion consequences of nanofluid in the permeable material. Bilal et al. [15] considered MHD second grade nanofluid flow induced by a rotatory cone. Anam et al. [16] investigated the assessment of nanofluid in a Von Karman flow with temperature relied viscosity. Zhu et al. [17] used a second-order slide in the nanofluid flow such as thermal radiation. Ramesh and its contributors have made a further contribution to the maxwell fluid-fluid velocity of nanoparticles over the permeable surface [18]. Khan and Pop [19] established boundary layer formulas for the viscous flow of nanofluid over-stretching surfaces. Kishan and Deepa [20] explored the results of nanofluid flow near the stagnation-point flow movement over linearly flowing medium in the presence of permeable material. Alim et al. [21] studied the flow of nanoparticles from over vertical disk embedded in a porous of Joule heat impact. Sheikholeslami et al. [22] studied the normal convention for the transport of heat in a sine wall cavity in the existence of Nanocomposites. In another attempt, Sheikholeslami and Ganji [23] proposed a statistical model for nanoparticles for both a single-phase and a two-phase fluid model.

Primarily, the phrase "bioconvection" was used by Platt [24] that is affiliated with streaming structures discovered in dense cultures of free-swimming micro-organisms. In isothermal drilling fluids swimming microorganisms when motile divers promote sustainable for the this dissipation phase, Kessler [25] demarcated heat transfer rhythms that could form impulsively. Gravitational influence and vorticity fix the routes of the atoms, culminating in cells tending toward the center of the fluid where the downward speed is high. This system of concentration is called a gyrotaxis. Kuznestsov [26] has studied the warming effect on the quality at a small depth of the gyrotaxic moving fluid. As a result of his research, it was shown that the suspended cells were less robust under the temperature effect opposed to the suspension under atmospheric pressure. Khan et al. [27] investigated a semi-analytical description of a provable non-linear transformation results from a 2D mixed convection system in which gravitational force non-Newtonian nanofluid films, including the viscoelastic fluid and gyrotactic microbes flow from Casson and Williamson through the thermal surface layer of the vertical shape, were investigated and the impact of boundary fluids was also investigated. They also discussed the effects on fluid flow of Boundary layer and thermophoresis forces. Zuhra et al. [28] explained the gyrotactic mechanism to use a porous medium curved wall with an MHD second-grade nanofluid flow under passively controlled nanofluid continuity equation. The research further examined the effect of parameters. On a porous surface fixed in a rubber mixture supplemented Newtonian heating, Mahdy [29] examined mixed convection flow with viscous dissipation arising from the nanofluid system. Standard coolant convection flow is suitable for cooling nuclear plants and explorers in the field. Shivraj et al. [30] shed research on the impact of microorganisms and thermal radiation on this same scale of nanostructures 29 nm in CuO skin friction-water nanofluid flow over the outer part of the dielectric resonator system, including the vehicle shield, the car upper part, the rocket upper point surface, etc. Khan et al. [31] developed numerical modeling and analysis of bioconvection on MHD flow due to an upper paraboloid surface of revolution. These authors also showed the influence of different parameters throughout plotted on the velocity area, temperature, concentration, and density of microorganism profiles. The mixed bioconvection flow of nanomaterials containing MHD microbiota from either a vertical type cylinder was explained by Rashad et al. [32], examining passively controlled nanofluid systems that are much more credible than organizations finding models in their work perspective. In a 3D steady flow model, Dimanche et al. [33] examined the nanofluid containing gyrotactic microbes and investigated the approximate results of the above model under the environment of an anisotropic slip next to a flow stream. He also demonstrated the influence of the activation force of Arrhenius, the heating jule, accompanying binary chemical processes. Recently, Li et al. [34]studied the bioconvection flow of modified second-grade nanofluids with thermal radiation and Wu's slip.

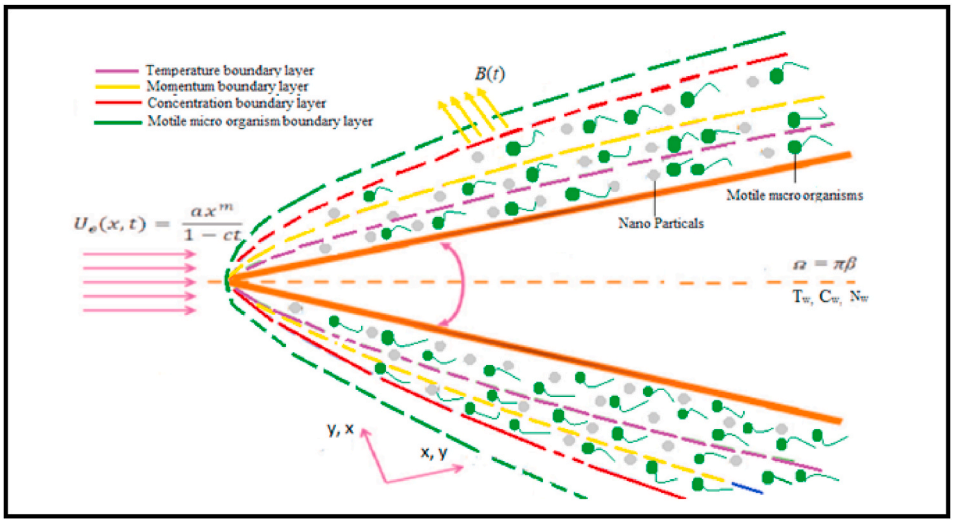

Fig. 1. Flow problem.

The above survey convinced to make a comprehensive investigation on thermal transporation of non Newtonian tangent hyperbolic fluid flow across an extending wedged surface. The fluid transportation is affected by non-Darcy porosity and magnetic field. Homogenous diffusion of nano particles and self motile microorganisms is considered in the base fluid. Effective constraints at the wedge wall include Wu's slip, zoro mass flux and convective boundary conditions. It is to evaluate, how do these boundary constraints along with other physical aspects of the study affect the profiles and surface gradients of fluid temperature, velocity, nano particles concentrartion and microorganism density. The set of the leading non linear, coupled differential equations in the presence of bioconvection is resolved numerically with implementation of matlab function bvp4c.

2. Mathematical modeling

2.1. The fluid model

There are several models in the research that explain the various rheological flow characteristics for fluids. Tangent hyperbolic is among the non-Newtonian fluid flow systems that can be used to explain the shear thinning performance, i.e. the viscosity reduces by growing the shear rate. The permeate flux ranges steadily from zero to the shear rate.

The constitutive of fluid written as

$$\tau = [\mu_\infty + (\mu_0 + \mu_\infty)\tanh(\Gamma\dot{\omega})^n]\dot{\omega} \tag{1}$$

where infinite shear rate viscosities $\dot{\omega}$, Γ is the time constant,n is the power-law index, τ is the extra stress tensor, $\mu_0$and μ_∞ represent zero respectively is expressed as

$$\dot{\omega} = \sqrt{\frac{1}{2}\sum \dot{\omega}_{ij}\,\dot{\omega}_{ji}} = \sqrt{\frac{1}{2}\prod}, \tag{2}$$

where

$$\prod = \frac{1}{2} tr\left[gradV + (gradV)^T\right]^2. \tag{3}$$

Consider the assumption $\mu_\infty = 0$. As we are focusing on the shear thinning behavior therefore for $\Gamma\dot{\omega} < 1$, the extra stress tensor τ is reduced to

$$\begin{aligned} \tau &= \mu_0[(\Gamma\dot{\omega})^n]\dot{\omega} = \mu_0[(1+\Gamma\dot{\omega}-1)^n]\dot{\omega} \\ \tau &= \mu_0[(1+N(\Gamma\dot{\omega}-1)^n)]\dot{\omega}, \end{aligned} \tag{4}$$

2.2. Problem formulation

In the existence of the magnetic field impact, the bioconvection with microorganisms for heat and mass movement of the tangent hyperbolic nanoparticles moving fluid a stretched wedge was scrutinized. The wedge is positioned in such a way that $x-axis$ coincides with the sheet of the wedge and the y-axis is taken perpendicular to the wedge surface as demonstrated in Fig. 1. The angle of the wedge is assumed to be $\Omega = \pi\beta$ where the Hartree pressure gradient $\beta = \frac{2m}{1+m}$. The stagnation point flow is time-dependent and the stretching velocity of the wedge is $U_\omega(x,t) = \frac{bx^m}{1-ct}$, the free stream velocity $U_e(x,t) = \frac{ax^m}{1-ct}$where b is a stretching rate and a, c, m are constants $0 \le m \le 1$. The u and v are velocity components. $B(t) = \frac{B_0}{(1-ct)^{1/2}}$is magnetic field. The surface fluid temperature is $T_w(x,t) = T_\infty + \frac{T_0 U_w x}{\nu(1-ct)^{1/2}}$ which is higher than the ambient temperature T_∞. The wedge is convectively heated with a heat transfer rate hf. The concentration nanomaterial at the surface is $C_w(x,t) = C_\infty + \frac{C_0 U_w x}{\nu(1-ct)^{1/2}}$ which is also higher than the ambient concentrationC_∞, $N_w(x,t) = N_\infty + \frac{N_0 U_w x}{\nu(1-ct)^{1/2}}$ is the surface concentration of motile microorganism. The initial reference temperature, the concentration of nanoparticles, and suspended microorganisms are denoted byT_0, $C_0$and N_0 respectively.

Because of the above assumptions, the governing equations are as follows [35,44]:

$$u_t + uu_x + vu_y = U_{et} + U_e U_{ex} + \nu\left((1-n) + \sqrt{2}\, n\Gamma u_y\right)u_{yy} - \frac{\sigma B_0^2}{\rho_f}(u - U_e) - \frac{\nu\phi}{K^*}(u - U_e) + \frac{1}{\rho_f}\begin{bmatrix}(1-C_f)\rho_f\beta g(T-T_\infty) - (\rho_p - \rho_f)g(C-C_\infty)\\ -(n-n_\infty)g\gamma(\rho_m - \rho_f)\end{bmatrix}, \tag{5}$$

$$T_t + uT_x + vT_y = \alpha\partial_y(T_y) + \Lambda\left(D_B C_y T_y + \frac{D_T}{T_\infty}(T_y)^2\right) - \frac{1}{(\rho C_p)}q_{r_y} \tag{6}$$

$$C_t + uC_x + vC_y = \frac{D_T}{T_\infty}\partial_y(T_y) + D_B\partial_y(C_y), \tag{7}$$

$$N_t + uN_x + vN_y + \frac{bW_c}{(C_w - C_\infty)}\left[\partial_y(NC_y)\right] = D_m(N_{yy}), \tag{8}$$

$$u_x + u_y = 0 \tag{9}$$

In equation (2) $q_r$is the Rosseland radiative heat flux and is defined as

$$q_r = -\frac{4\sigma^*}{3k^*}T_y^4 \tag{10}$$

where $\sigma^*$is the Stefan-Boltzmann constant and $k^*$is the mean absorption coefficients. By using series expansion aboutT_∞, T_4 can be expressed as

$$T^4 = T_\infty^4 + 4T_\infty^3(T - T_\infty) + 6T_\infty^2(T - T_\infty)^2 + \ldots \tag{11}$$

$$T_t + uT_x + vT_y = \left(\alpha_0 + \frac{16\sigma_s T_\infty^3}{3k^*}T_{yy}\right)T_{yy} + \Lambda\left(D_B C_y T_y + \frac{D_T}{T_\infty}(T_y)^2\right) \tag{12}$$

The associated boundary conditions:

$$\left.\begin{aligned} &u = U_w + U_{slip}, v = 0, -kT_y = h_f(T_w - T), D_B C_y + \frac{D_B}{T_\infty}T_y = 0,\ N = N_w(x,t) \quad at\ y = 0,\\ &u \to U_e, \quad T \to T_\infty,\ C \to C_\infty,\ N \to N_\infty \quad as \quad y \to \infty \end{aligned}\right\}, \tag{13}$$

where Wu's slip velocity U_{slip} (see Ref. [36]) and Knudsen numberK_n [37–39] are taken as below:

$$U_{slip} = \frac{2}{3}\left(\frac{3-\alpha l^2}{\alpha} - \frac{3}{2}\frac{1-l^2}{K_n}\right)B_1 u_y - \frac{1}{4}\left[l^4 + \frac{2}{K_n^2}(1-t^2)\right]B_1^2 u_{yy},\ U_{slip} = A_1 u_y + u_{yy} \tag{14}$$

where A_1 and B_1 are constant, $l = \min\left(\frac{1}{K_n}, 1\right)$,momentum accommodation coefficient α for $0 \le \alpha \le 1$, and molecular mean free path β_1. First order velocity slip γ, second-order velocity slip δ. The based on the definition l, it is noticed that for any given value of the K_n, here $0 \le l \le 1$. Moreover, we know that $\beta_1 < 0$ and hence the second term in the right-hand side of equation (11) is a positive number.

In the above expretion the density is ρ_f, fluid specific heat $(C_p)_f$, electrical conductivity σ, density of the nanomatirials ρ_p, α the thermal diffusivity, power-law index n, Λ is the ratio of the specific heat, thermal conductivity k, and the specific hea tC_p. In addition,D_T thermophoresis and D_BBrownian motion.

To make the above governing equations dimensionless, the following transformations [35] have been introduced.

$$\left.\begin{aligned}&\zeta = y\sqrt{\frac{(m+1)U_e}{2\nu x}}, \theta(\zeta) = \frac{(T-T_\infty)}{(T_w-T_\infty)}, \varphi(\zeta) = \frac{(C-C_\infty)}{(C_w-C_\infty)},\\ &\chi(\zeta) = \frac{(N-N_\infty)}{(N_w-N_\infty)}, \psi = f(\zeta)\sqrt{\frac{2\nu x U_e}{m+1}},\end{aligned}\right\} \tag{15}$$

After simplification, equations (5)–(8) yield the following ODEs whereas eq. (9) is satisfied identically:

$$(1-n+nWef'')f''' - A\left(\frac{1}{2}\eta f'' + f' - 1\right)(2-\beta) - \beta\left(f'2-1\right) + ff'' - K_1(f'-1)$$
$$(2-\beta) + \lambda(\theta - Nr\varphi - Nc\chi) = 0, \tag{16}$$

$$\left(1+\frac{4}{3}Rd\left(\begin{matrix}1+\\(\theta_w-1)\theta^3\end{matrix}\right)\right)\theta'' + \Pr\left(f\theta' - 2f'\theta) - \frac{A}{2}(\eta\theta' + 3\theta)(2-\beta) + Nb\theta'\varphi' + Nt\theta'^2\right) = 0 \tag{17}$$

$$\varphi'' + \Pr Le\left(-\frac{A}{2}(\eta\varphi' + 3\varphi)(2-\beta) + (f\varphi' - 2f'\varphi)\right) + \frac{Nt}{Nb}\theta'' = 0 \tag{18}$$

$$\chi'' + Lbf\chi' - Pe(\varphi''(\chi+\delta_1) + \chi'\varphi') = 0. \tag{19}$$

with

$$\left.\begin{aligned}&f(\zeta) = 0, f'(\zeta) = 1 + \gamma f''(0) + \delta f'''(0), \chi(\zeta) = 1,\\ &\theta'(\zeta) = -\gamma(2-\beta)^{1/2}(1-\theta), Nb\varphi'(\zeta) + Nt\theta'(\zeta) = 0, at\ \zeta = 0,\\ &f'(\zeta)\to 1, \theta(\zeta)\to 0, \varphi(\zeta)\to 0, \chi(\zeta) = 0,\ as\ \zeta\to\infty.\end{aligned}\right\} \tag{20}$$

In the above equations, $M = \frac{\sigma B_0^2}{a\rho x^{m-1}}$ magnetic parameter, $We = \frac{\sqrt{\Gamma^2(m+1)U_e^3}}{\nu x}$ is the Weissenberg number, $\Pr = \frac{\nu}{\alpha}$ denotes the Prandtl number, K_1 is combined magnetic porosity number, $Ec = \frac{U_w^2}{(\sigma_p)_f(T_w-T_\infty)}$ is Eckert number, $Le = \frac{\alpha}{D_B}$ is Lewis number, $Nt = \frac{\Lambda D_T(T_w-T_\infty)}{T_\infty\nu}$is thermophoresis parameter, $Rd = \frac{4\sigma^* T_\infty^3}{kk^*}$ is thermal radiation parameter, $\mathrm{Re}_x = \frac{xU_e}{\nu}$is Reynolds number, $Nb = \frac{\Lambda D_B(C_w-C_\infty)}{\nu}$is the Brownian motion parameter, $A = \frac{c}{ax^{m-1}}$is unsteadiness parameter, $\lambda = \frac{U_w}{U_e}$ is the velocity ratio parameter and $\gamma = \frac{h_f}{k}x\mathrm{Re}^{-1/2}$ is the generalized Biot number, and $\theta_w\left(=\frac{T_w}{T_\infty}\right)$ is temperature ratio parameter.

Here the physical quantities of engineering importance namely $-f''(0)$, $-\theta'(0)$, $\varphi'(0)$ and $-\chi'(0)$ are defined as

$$\left.\begin{aligned}&C_f = \frac{T_w}{\rho_f U_w^2}, Nu = \frac{xq_w}{k(T_w-T_\infty)}, Sh = \frac{xj_w}{D_B(C_w-C_\infty)}, Nh = \frac{xg_w}{D_B(N_w-N_\infty)}\end{aligned}\right\}, \tag{21}$$

Here τ_w is shear stress, q_w is heat flux, j_w is the mass flux of nano entities and g_w is the mass flux of microorganisms.

$$\left.\begin{aligned}&\tau_w = \mu\left((1-n)\frac{\partial u}{\partial y} + \frac{n\Gamma}{\sqrt{2}}\left(\frac{\partial u}{\partial y}\right)^2\right)_{y=0},\\ &q_w = -k\left(\left(1+\frac{16\sigma^* T_\infty}{3kk^*}\right)\frac{\partial T}{\partial y}\right)_{y=0},\\ &j_w = -D_B\left(\frac{\partial C}{\partial y}\right)_{y=0}, g_w = -D_B\left(\frac{\partial N}{\partial y}\right)_{y=0}\end{aligned}\right\}, \tag{22}$$

In dimensionless form are

$$\left.\begin{aligned}&C_f\mathrm{Re}_x^{1/2}\sqrt{\frac{2}{m+1}} = (1-n)f''(0) + \frac{n}{2}We(f''(0))^2,\\ &Nu_x\mathrm{Re}_x^{1/2}\sqrt{\frac{2}{1+m}} = -\left(1+\frac{4}{3}Rd\right)\theta'(0),\\ &Sh_x\mathrm{Re}_x^{-1/2}\sqrt{\frac{2}{1+m}} = -\varphi'(0),\\ &Nh_x\mathrm{Re}_x^{-1/2}\sqrt{\frac{2}{1+m}} = -\chi'(0),\end{aligned}\right\}, \tag{23}$$

Here $\mathrm{Re}_x = \frac{xU_e}{\nu}$ is Reynolds number.

Table 1
Enumeration of comparative findings of skin friction factor. $-f''(0)$

β	Rajagopal et al. [40]	Kuo [41]	Ishak et al. [42]	Atif et al. [43]	Present Results
0.0	–	0.469600	0.4696	0.4696	0.469600
0.1	0.587035	0.587080	0.5870	0.5870	0.587035
0.3	0.774755	0.774724	0.7748	0.7747	0.774757
0.5	0.927080	0.927005	0.9277	0.9270	0.927081
1	1.2322585	1.232258	1.23226	1.23225	1.2322588

Table 2
Numerical estimation of $-f''(0)$ via physical parameters.

A	M	β	We	n	λ	Nr	Nc	$-f''(0)$
0.1	1.0	0.5	0.3	0.2	0.1	0.5	0.5	1.5648
0.3								1.5496
0.4								1.5421
0.2	**0.5**	0.5	0.3	0.2	0.1	0.5	0.5	1.3383
	1.5							1.7376
	2.0							1.8926
0.2	1.0	**0.2**	0.3	0.2	0.1	0.5	0.5	1.5656
		0.4						1.5595
		0.6						1.5552
0.2	1.0	0.5	**2.0**	0.2	0.1	0.5	0.5	1.6755
			3.0					1.7483
			4.0					1.8234
0.2	1.0	0.5	0.3	**0.1**	0.1	0.5	0.5	1.4764
				0.3				1.6500
				0.5				1.8915
0.2	1.0	0.5	0.3	0.2	**0.2**	0.5	0.5	1.5555
					0.4			1.5524
					0.6			1.5494
0.2	1.0	0.5	0.3	0.2	0.1	**1.0**	0.5	0.9205
						2.0		0.9170
						3.0		0.9136
0.2	1.0	0.5	0.3	0.2	0.1	0.5	**1**	0.9333
							2	0.9557
							3	0.9785
0.1	1.0	0.5	0.3	0.2	0.1	0.5	0.5	1.5648
0.3								1.5496
0.4								1.5421

$$
\left.
\begin{aligned}
y_1' &= y_2 \\
y_2' &= y_3 \\
y_3' &= \frac{1}{1-n+nWey_3}\left(\begin{array}{l}\Big(2-\beta\Big)A\Big(\frac{\zeta}{2}y_3+y_2-1\Big)+\beta\Big(y_2^2-1\Big)-y_1y_3 \\ \\ +K_1(2-\beta)(y_2-1)-\lambda(\mathrm{y_5}-\mathrm{Nry_7}-\mathrm{Ncy_9}\end{array}\right), \\
y_4' &= y_5, \\
y_5' &= \frac{1}{\mathrm{Pr}_{eff}}\left(y_1y_5-2y_2y_4-\frac{A}{2}(2-\beta)(\zeta y_5-3y_4)+Nby_5y_7+Nty_5^2\right), \\
y_6' &= y_7, \\
y_7' &= \mathrm{Pr}Le\left(\frac{A}{2}(2-\beta)(\zeta y_7-3y_6)-(y_1y_7-2y_2y_6)\right)-\frac{Nt}{Nb}y_5', \\
y_8' &= y_9, \\
y_9' &= -Lby_1y_{10}-0.5A(2-\beta)(\zeta y_9-3y_8)+Pe(y_8y_{10}+dy_8(y_9+\delta_1))
\end{aligned}
\right\}, \tag{24}
$$

Table 3
Numerical estimation of $-\theta'(0)$ via physical parameters.

A	β	Le	Nt	Nb	Pr	γ	λ	$-\theta'(0)$
0.1	0.5	5.0	0.5	0.2	1.2	0.1	0.1	0.3620
0.3								0.3948
0.4								0.4054
0.2	**0.2**	5.0	0.5	0.2	1.2	0.1	0.1	0.2032
	0.4							0.3326
	0.6							0.4221
0.2	0.5	**1.0**	0.5	0.2	1.2	0.1	0.1	0.3824
		6.0						0.3811
		10						0.3808
0.2	0.5	5.0	**0.2**	0.2	1.2	0.1	0.1	0.3825
			0.4					0.3817
			0.6					0.3809
0.2	0.5	5.0	0.5	**0.3**	1.2	0.1	0.1	0.3813
				0.4				0.3814
				0.6				0.3815
0.2	0.5	5.0	0.5	0.2	**3.0**	0.1	0.1	0.4589
					5.0			0.4948
					7.0			0.5153
0.2	0.5	5.0	0.5	0.2	1.2	**0.2**	0.1	0.3735
						0.3		0.3672
						0.5		0.3575
0.2	0.5	5.0	0.5	0.2	1.2	0.1	**0.2**	0.3813
							0.4	0.3816
							0.6	0.3819

Table 4
Numerical estimation of $\varphi'(0)$ via physical parameters.

Pr	Rd	Nt	Nb	A	β	γ	λ	$\varphi'(0)$
3.0	0.2	1.0	0.2	0.2	0.5	0.1	0.1	1.1472
5.0								1.2370
7.0								1.2883
1.0	**2.0**	1.0	0.2	0.2	0.5	0.1	0.1	0.8576
	3.0							0.7892
	4.0							0.7366
1.0	0.2	**0.2**	0.2	0.2	0.5	0.1	0.1	0.3825
		0.4						0.7633
		0.6						1.1426
1.0	0.2	1.0	**0.3**	0.2	0.5	0.1	0.1	0.6355
			0.4					0.4766
			0.6					0.3177
1.0	0.2	1.0	0.2	**0.1**	0.5	0.1	0.1	0.9050
				0.4				0.9869
				0.6				1.0136
1.0	0.2	1.0	0.2	0.2	**0.2**	0.1	0.1	0.5080
					0.4			0.8316
					0.6			1.0552
1.0	0.2	1.0	0.2	0.2	0.5	**0.2**	0.1	0.9338
						0.4		0.9181
						0.6		0.8939
1.0	0.2	1.0	0.2	0.2	0.5	0.1	**0.2**	0.9532
							0.4	0.9539
							0.6	0.9546

Table 5
Numerical estimation of $-\chi^{'}(0)$ via physical parameters.

Nt	*Nb*	*M*	*We*	Pr	*n*	*Nr*	*Nc*	σ	*Le*	λ	*Pe*	β	$-\chi^{'}(0)$
0.2	0.2	1.0	0.3	1.2	0.2	0.5	0.5	0.1	5.0	0.1	0.1	0.5	1.1192
0.4													1.0877
0.6													1.0563
0.5	**0.3**	1.0	0.3	1.2	0.2	0.5	0.5	0.1	5.0	0.1	0.1	0.5	1.0983
	0.4												1.1115
	0.6												1.1246
0.5	0.2	**0.5**	0.3	1.2	0.2	0.5	0.5	0.1	5.0	0.1	0.1	0.5	1.0966
		1.5											1.0533
		2.0											1.0390
0.5	0.2	1.0	**2.0**	1.2	0.2	0.5	0.5	0.1	5.0	0.1	0.1	0.5	1.0595
			3.0										1.0525
			4.0										1.0455
0.5	0.2	1.0	0.3	**3**	0.2	0.5	0.5	0.1	5.0	0.1	0.1	0.5	1.0474
				5									1.0355
				7									1.0286
0.5	0.2	1.0	0.3	1.2	**0.1**	0.5	0.5	0.1	5.0	0.1	0.1	0.5	1.0803
					0.3								1.0622
					0.5								1.0397
0.5	0.2	1.0	0.3	1.2	0.2	**1.0**	0.5	0.1	5.0	0.1	0.1	0.5	1.0721
						2.0							1.0722
						3.0							1.0724
0.5	0.2	1.0	0.3	1.2	0.2	0.5	**1**	0.1	5.0	0.1	0.1	0.5	1.0680
							2						1.0598
							3						1.0513
0.5	0.2	1.0	0.3	1.2	0.2	0.5	0.5	**0.2**	5.0	0.1	0.1	0.5	1.0653
								0.4					1.0519
								0.6					1.0385
0.5	0.2	1.0	0.3	1.2	0.2	0.5	0.5	0.1	**1.0**	0.1	0.1	0.5	1.0772
									6.0				1.0713
									10				1.0695
0.5	0.2	1.0	0.3	1.2	0.2	0.5	0.5	0.1	5.0	**0.2**	0.1	0.5	1.0720
										0.4			1.0726
										0.6			1.0732
0.5	0.2	1.0	0.3	1.2	0.2	0.5	0.5	0.1	5.0	0.1	**0.2**	0.5	0.9275
											0.3		0.8558
											0.4		0.7847
0.5	0.2	1.0	0.3	1.2	0.2	0.5	0.5	0.1	5.0	0.1	0.1	**0.2**	1.1073
												0.4	1.0814
												0.6	1.0635

2.3. Numerical method

The system of the nonlinear differential equations (16-19) subject to boundary conditions (20) is resolved numerically by using the Matlab function bvp4c. In the above-mentioned equations, the higher-order derivatives are reduced to first-order as follows:

with

$$\left.\begin{array}{l} y_1(\zeta)=0, y_2(\zeta)=\lambda, y_5(\zeta)=-\gamma(2-\beta)^{1/2}(1-y_4(\zeta)), \\ y_6(\zeta)=1,\ as\ \zeta=0, y_2(\zeta)\to 1, y_4(\zeta)\to 0, y_6(\zeta)\to 0, \\ as\ \zeta\to\infty \end{array}\right\} \tag{25}$$

This first-order system of differential equations is coded on Matlab platform and computational endeavor is continued for the suitable ranges of the pertinent parameters to elucidate their impacts on the velocity, $f^{'}(\zeta)$, temperature profile $\theta(\zeta)$, concentration profile $\varphi(\zeta)$ and the $\chi(\zeta)$, skin friction coefficient, local Nusselt number, motile organism density number.

2.3.1. Tabular results and discussion

Table 1 presents the comparison of our results with previously reported data available in the literature. An acceptable accord among the two sets of results establishes the validly of the numerical method being implemented herein. Table 2 indicated that the skin friction coefficient $-f''(0)$is declined when each of the parameters*A*, $\beta\lambda$, *Nr* are incremented but it is enhanced when the parameters*M*, *We*, *n*, λ, *Nc* are boosted. The estimation of $-\theta^{'}(0)$ rises directly with *A*, β, P_r but its value depreciates against mounting γ as enumerated in Table 3. The other parameters did not show any significant result on $-\theta^{'}(0)$. Table 4 demonstrate the variation of $\varphi^{'}(0)$ with relation to various parameters. The quantity $\varphi^{'}(0)$shows increasing trend when each of P_r, N_tA, *M*, β are enhanced but it is decreased with

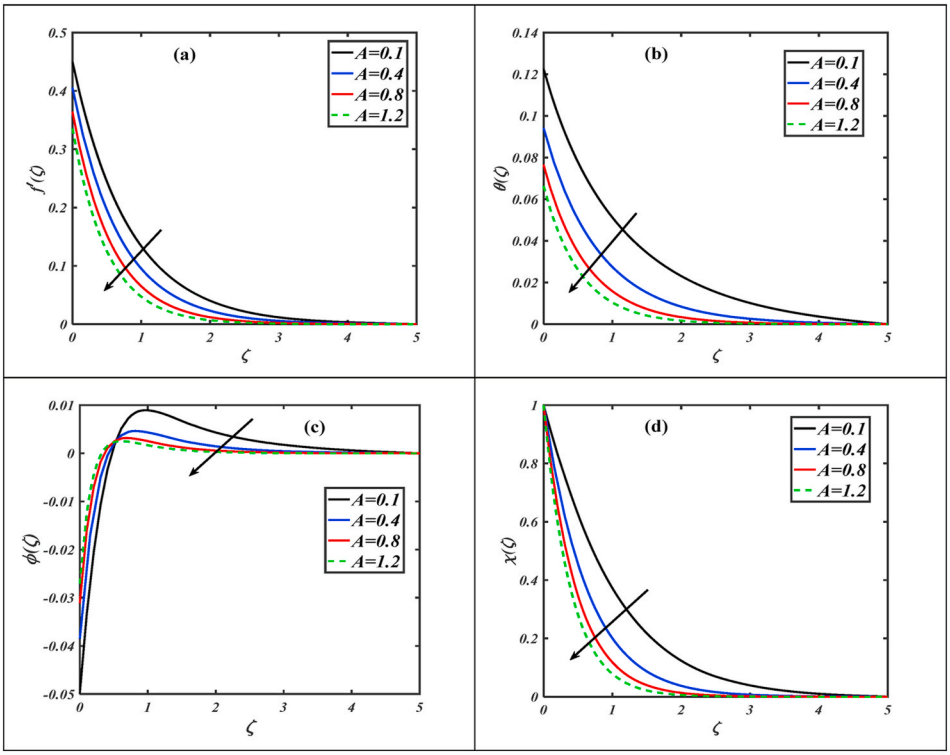

Fig. 2. Plots of $f'(\zeta)$, $\theta(\zeta)$, $\varphi(\zeta)$ and $\chi(\zeta)$ with variation of A.

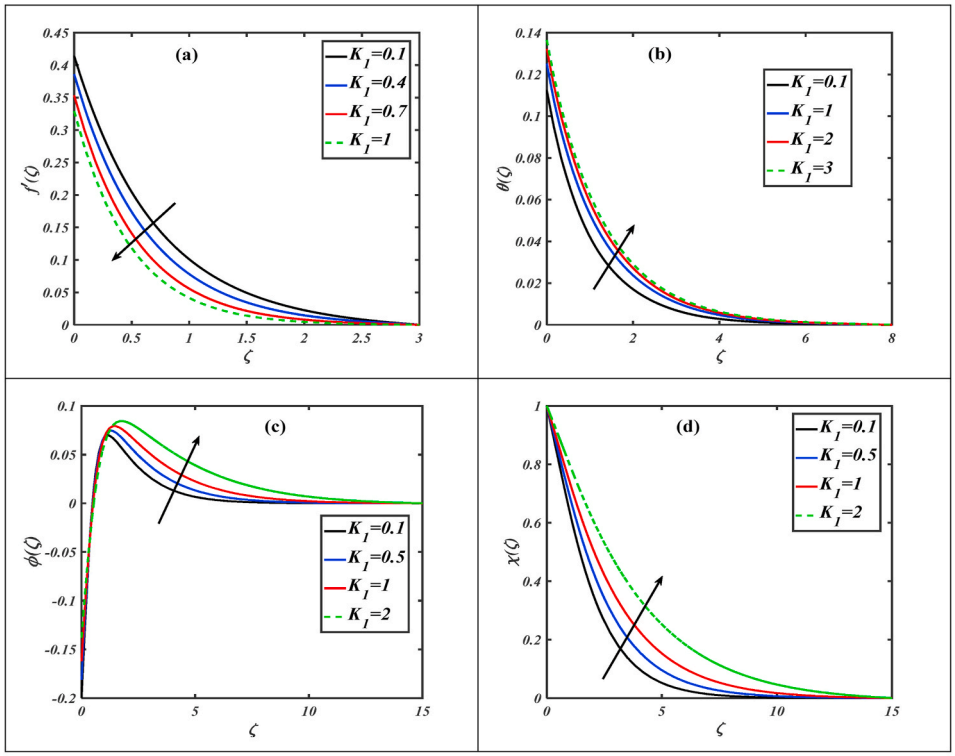

Fig. 3. Plots of $f'(\zeta)$,$\theta(\zeta)$, $\varphi(\zeta)$and $\chi(\zeta)$ with variation of K_1

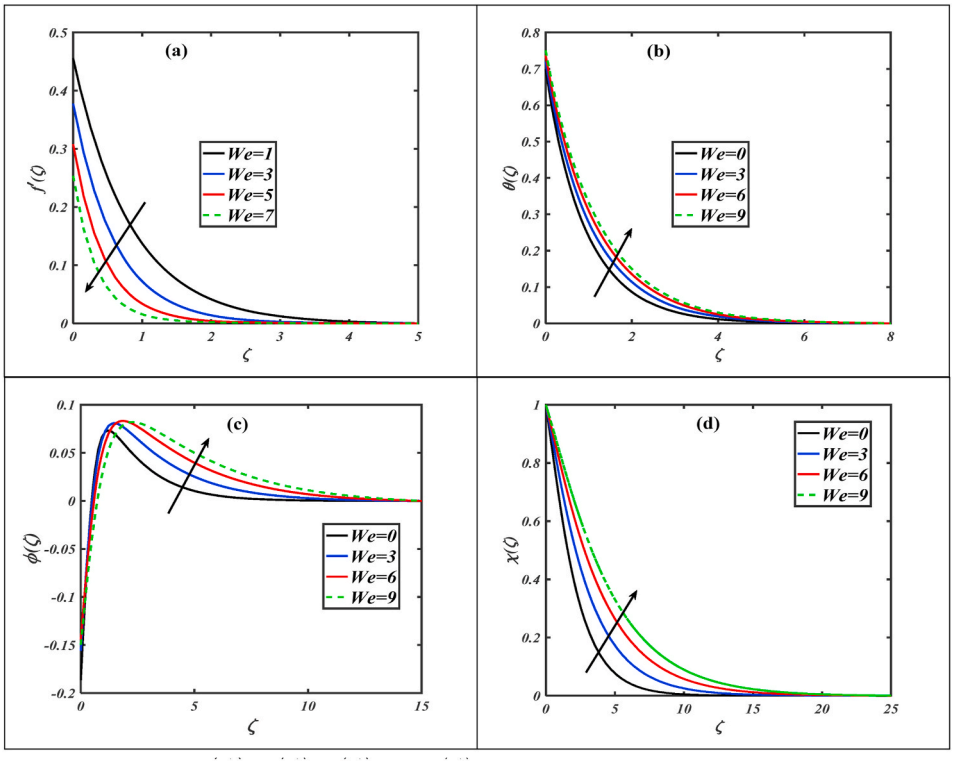

Fig. 4. Plots of $f'(\zeta)$,$\theta(\zeta)$, $\varphi(\zeta)$and $\chi(\zeta)$ with variation of.*We*

increment in the values of R_d, $N_b$and γ. The motile organism density number $-\chi'(0)$become lesser when N_t, n, δ are incremented but it becomes larger with $N_b$as noticed in Table 5.

Comparison.

3. Results and discussion

This segment pertains to pictoral representation of the out puts yielded from the numeric solution of the problem being studied. Fig. 2(a–d) illustrate the impact of the unsteadiness parameter A, on the $f'(\zeta)\theta(\zeta)$, $\varphi(\zeta)$and $\chi(\zeta)$ profiles. The increase in the value of unsteadiness parameter A means laps of time after stretching jerk which resulted in straight reduction of velocity, temperature and microorganism density but the graph of nano particle concentration is increasing function of values of A and then these graphs become asymptotic to the value zero as $\zeta \to \infty$. Fig. 3(a–d) demonstrate the effects of the combined magnetic and the porosity parameter K_1 on the physical quantities $f'(\zeta)$, $\theta(\zeta)$, $\varphi(\zeta)$ and $\chi(\zeta)$. The parameter K_1 is proportional to magnetic field strength and inversely related to permeability of porous medium, hence its increasing value indicates the more resistive force against the flow field which reduces the velocity but causes increase in each of $\theta(\zeta)$, $\varphi(\zeta)$and $\chi(\zeta)$. Thus, both Lorentz force associated with magnetic parameter and presence of permeability of porous medium boost up temperature, concentration and microorganism concentration profiles and their associated boundary layers. Similar behavior of the earlier mention four physical quantities can be observed in Fig. 4(a–d) under the increasing influence of Weissenberg number *We,* the ratio of the relation of the specific process time and the relaxation time of the fluid. The velocity ratio parameter λ depicted results opposite to K_1 and *We* as delineated in Fig. 5(a–d). The velocity profile is reduced and thinning of the boundary layer can be depicted in Fig. 6. (a) when the Power-law index n is incremented. Furthermore, the diagram for the velocity distribution is inclined to zero as$\zeta \to \infty$. As seen in Fig. 6(b–d), the temperature, concentration of nanomaterials and microorganism density functions are gradually increased with larger inputs of n. The increment in slip parameter γmarked reduction in flow speed $f'(\zeta)$ but it enhanced the quantities$\theta(\zeta)$, $\varphi(\zeta)$and $\chi(\zeta)$as exhibited in Fig. 7(a–d). It is because the slowing flow enhances the diffusion of energy and mass concentration. The temperature, and nanoparticles concentration rise up rapidly with increment in thermophoresis parameter N_t, the results are shown in Fig. 8(a–b). The thermopherotic effect causes the transportation of nano entities from regime of high temperature to that of lower one. As a consequence of this effect, the diffusion of thermal energy and concentration are improved. The effects of bioconvection Rayleigh number *Nc* on $\varphi(\zeta)$ and $\chi(\zeta)$are displayed in Fig. 8(c–d). Both the concentration of nanoparticles and density of the motile microorganisms are increasing functions of *Nc*.

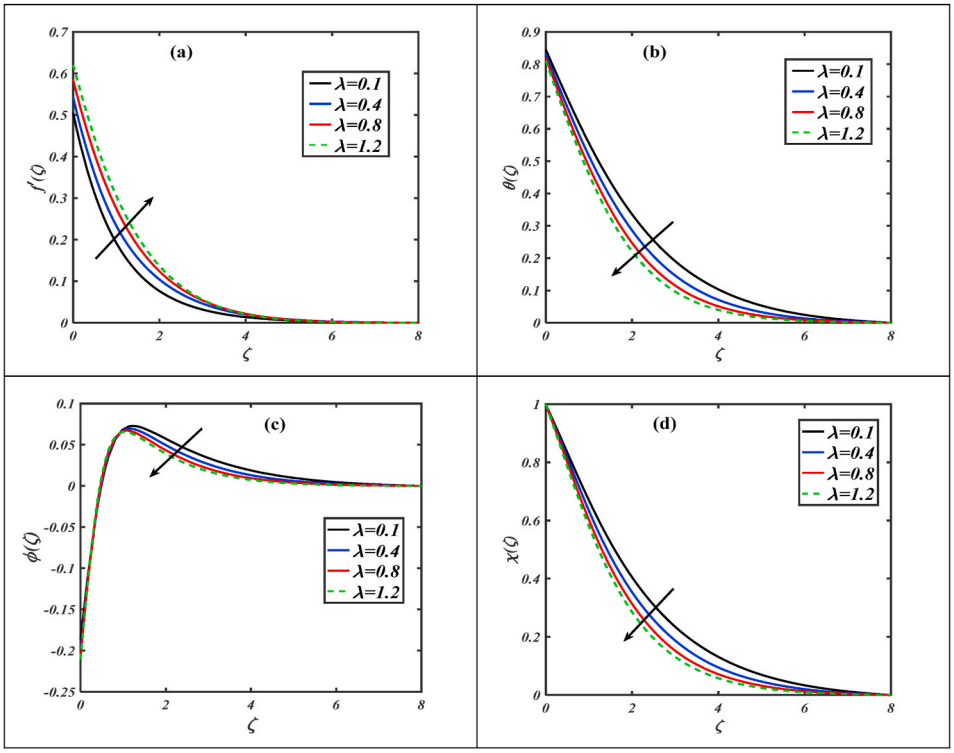

Fig. 5. Plots of $f'(\zeta)$,$\theta(\zeta)$, $\varphi(\zeta)$and $\chi(\zeta)$ with variation of λ

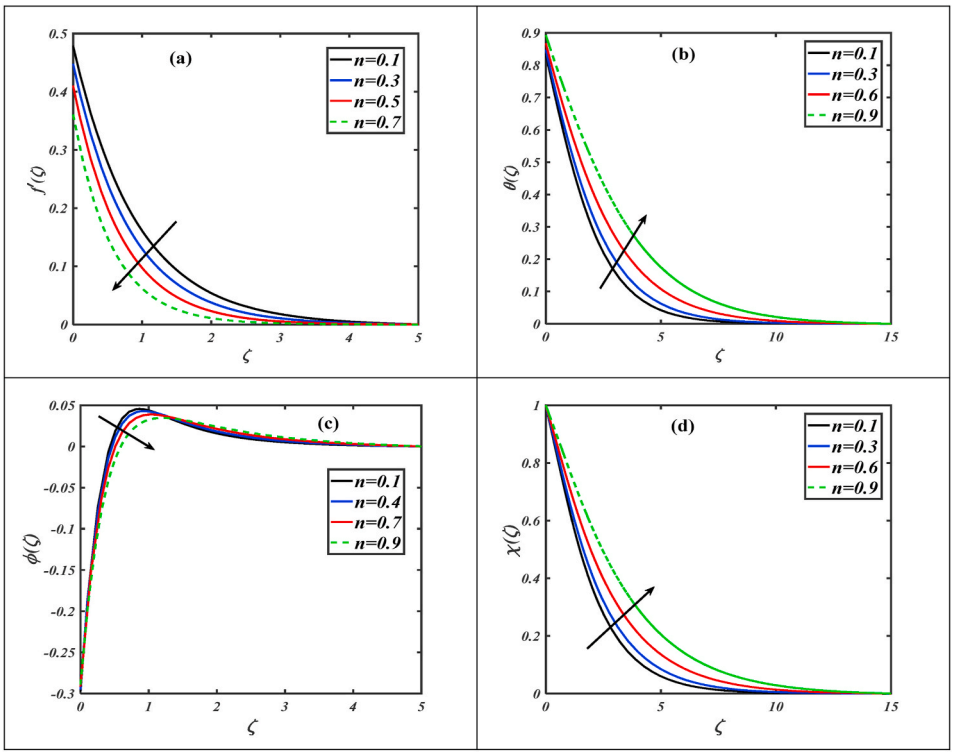

Fig. 6. Plots of $f'(\zeta)$,$\theta(\zeta)$, $\varphi(\zeta)$and $\chi(\zeta)$ with variation of power index parameter n.

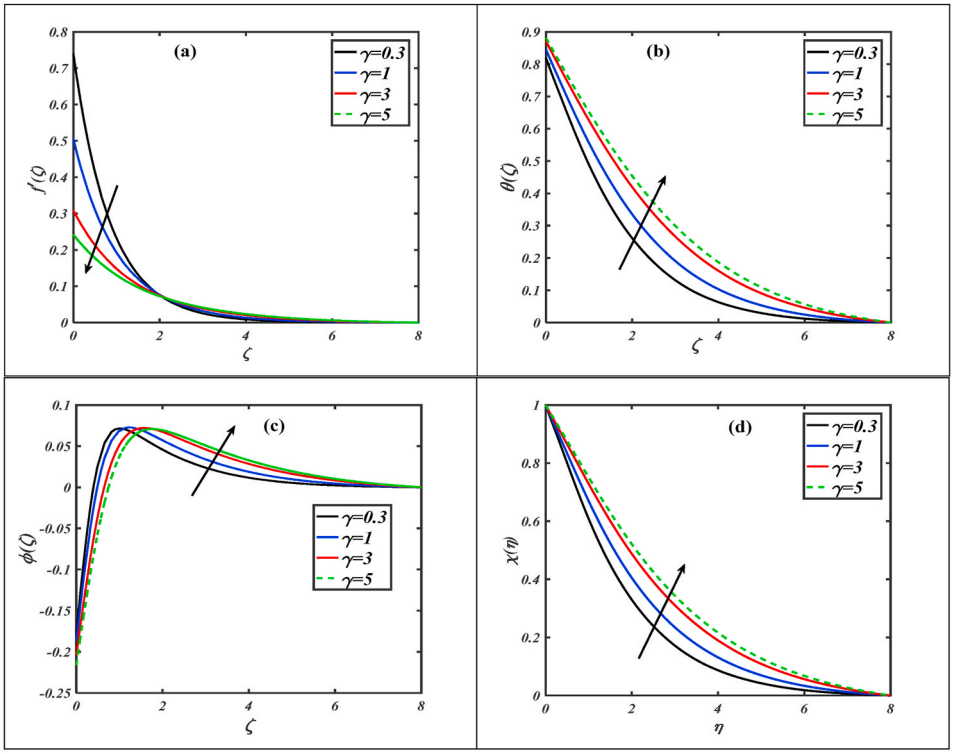

Fig. 7. Plots of $f'(\zeta)$, $\theta(\zeta)$, $\varphi(\zeta)$and $\chi(\zeta)$ with variation of slip parameter.γ

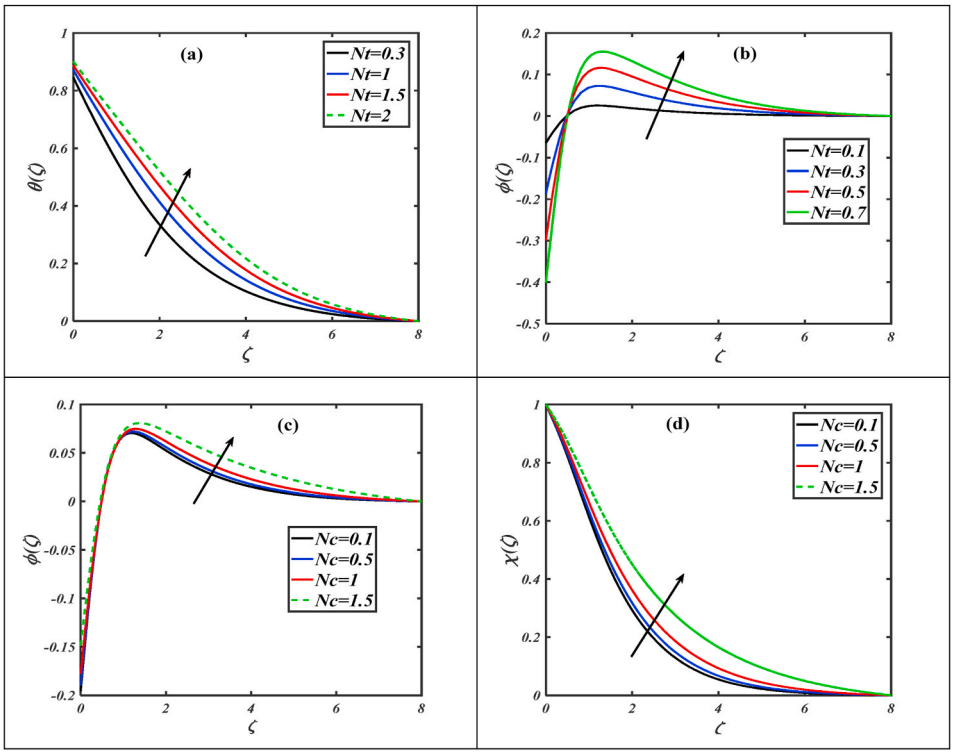

Fig. 8. Plots of $\theta(\zeta)$, $\varphi(\zeta)$and $\chi(\zeta)$ with variation of N_t and Nc.

4. Final remarks

This research explores the time-dependent heat transport phenomena for the MHD flow of nanofluids containing nanomaterials and motile microorganisms via porous matrix. The fluid flows flow through a porous stretched wedge with second-order slip and Nield boundary. The key points are listed below as:

- ♣ The velocity profile is accelerated for the higher variation of λ while it is depressed against the estimation of $A$and K_1.
- ♣ The velocity profile is also decreased for the greater values of $\gamma$and n.
- ♣ The temperature profile is boosted for the higher variation of Bi while it is declined against Prandλ .
- ♣ The concentration profile is increased for the higher variation of $Nr$and γ while the depressed for the estimation of Pr.
- ♣ The temperature profile is boosted for the higher variation of γ while the declined for the estimation of Peand Lb.

Author statement

Farooq Ahmad: Conceptualized the problem. Sajjad Hussain: Conceptualized the problem, wrote the original draft. MY Malik: validated the results of the problem by using different methods. Hassan Waqas: provided the data and resources. Hela Ayed: wrote the reviewed manuscript. M. Mossa Al-Sawalha: wrote the reviewed manuscript

Declaration of competing interest

The authors declare that they have no known competing financial interests or personal relationships that could have appeared to influence the work reported in this paper.

Acknowledgement

“This research has been funded by Scientific Research Deanship at University of Ha’il, Ha’il, Saudi Arabia through project number RG-20 081”.

References

[1] J.F. Morris, A review of microstructure in concentrated suspensions and its implication for rheology and bulk flow, Rheol. Acta 48 (2009) 909–923.
[2] A. Ya, Malkin, Non-Newtonian viscosity in steady-state shear flows, J. Non-Newton. Mech. 192 (2013) 48–65.
[3] A. Hussain, R. Zetoon, S. Ali, M.Y. Malik, Non-Newtonian squashed flow simulation across Darcy-Forchheimer sensor, Heat Tran. Asian Res. 48 (1) (2019) 398–413.
[4] T. Hayat, S. Ali, M. Awais, A. Alsaaedi, Joule heating effects on MHD flow of Burgers’ fluid, Heat Tran. Res. 47 (2016) 1083–1092.
[5] R.J. Moitsheki, T. Hayat, M.Y. Malik, F.M. Mahomed, Symmetry analysis for the nonlinear model of diffusion and reaction in porous catalysts, Nonlinear Anal. R. World Appl. 11 (4) (2010) 3031–3036.
[6] N.S. Akbar, S. Nadeem, R.U. Haq, Z. Khan, Numerical solutions of Magnetohydrodynamic boundary layer flow of tangent hyperbolic fluid towards a stretching sheet, Indian J. Phys. 87 (11) (2013) 1121–1124.
[7] U. Ali, M.Y. Malik, A.A. Alderremy, S. Aly, Rehman Ku, A generalized findings on thermal radiation and heat generation/absorption in nanofluid flow regime, Phys. Stat. Mech. Appl. 553 (2020) 124026, https://doi.org/10.1016/j.physa.2019.124026.
[8] M. Khan, T. Salahuddin, M.Y. Malik, A. Tanveer, A. Hussain, AS Alqahtani, 3-D axisymmetric Carreau nanofluid flow near the Homann stagnation region along with chemical reaction: application Fourier’s and Fick’s laws, Math. Comput. Simulat. 170 (2020) 221–235, https://doi.org/10.1016/j.matcom.2019.10.019.
[9] M. Naseer, M.Y. Malik, S. Nadeem, A. Rehman, The boundary layer flow of hyperbolic tangent fluid over a vertical exponentially stretching cylinder, Alex Eng J 53 (3) (2014) 747–750.
[10] T. Salahuddin, M.Y. Malik, A. Hussain, S. Bilal, M. Awais, Effects of transverse magnetic field with variable thermal conductivity on tangent hyperbolic fluid with exponentially varying viscosity, AIP Adv. 5 (12) (2015) 127103.
[11] S.U.S. Choi, Enhancing thermal conductivity of fluids with nanoparticles, Int. Mech. Eng. Cong. Exp., ASME, FED 231/MD 66 (1995) 99–105.
[12] J. Buongiorno, Convective transport in nanofluids, J. Heat Tran. 128 (2006) 240–250.
[13] W.A. Khan, I. Pop, Boundary-layer flow of a nanofluid past a stretching sheet, Int. J. Heat Mass Tran. 53 (2010) 2477–2483.
[14] M.M. Bhatti, M.M. Rashidi, Effects of thermo-diffusion and thermal radiation on Williamson nanofluid over a porous shrinking/stretching sheet, J. Mol. Liq. 21 (September) (2016) 567–573.
[15] S. Bilal, Zubair Mustafa, Khalil Ur Rehman, M.Y. Malik, Journal of Nanofluids , MHD Second Grade NanoFluid Flow Induced by a Rotatory Cone 8 (4) (2019) 876–884.
[16] A. Tanveer, T. Salahuddin, M. Khan, A.S. Alshomrani, M.Y. Malik, The assessment of nanofluid in a Von Karman flow with temperature relied viscosity, Res. Phys. 9 (2018) 916–922.
[17] Z. Jing, Z. Liu, Z. Liancun, Z. Xinxin, Second-order slip MHD flow and heat transfer of nanofluids with thermal radiation and chemical reaction, Appl. Math. Mech. -Engl. Ed. 36 (9) (2015) 1131–1146.
[18] G.K. Ramesh, B.J. Gireesha, T. Hayat, A. Alsaedi, Stagnation point flow of Maxwell fluid towards a permeable surface in the presence of nanoparticles, Alexandria Engineering Journal 55 (2) (2016) 857–865.
[19] W.A. Khan, I. Pop, Boundary-layer flow of a nanofluid past a stretching sheet, Int. J. Heat Mass Tran. 53 (2010) 2477–2483.
[20] N. Kishan, G. Deepa, Viscous dissipation effects on stagnation point flow and heat transfer of a micropolar nanofluid with uniform suction or blowing, Adv. Appl. Sci. Res. 3 (2012) 430–439.
[21] M.A. Alim, M.M. Alam, A.A. Mamun, B. Hossain, Combined effect nanofluid flow of viscous dissipation and Joule heating on the coupling of conduction and free convection along a vertical flat plate, Int. Commun. Heat Mass Tran. 35 (2008) 338–346.
[22] M. Sheikholeslami, M. Hatami, D.D. Ganji, Nanofluid flow and heat transfer in a rotating system in the presence of a magnetic field, J. Mol. Liq. 190 (2014) 112–120.
[23] M. Sheikholeslami, D.D. Ganji, Nanofluid flow and heat transfer between parallel plates considering Brownian motion using DTM, Comput. Methods Appl. Mech. Eng. 283 (2015) 651–663.
[24] J.R. Platt, Bioconvection patterns in cultures of free-swimming microorganisms, Science 133 (1963) 1766–1767.

[25] J.O. Kessler, Gyrotactic buoyant convection and spontaneous pattern formation in algal cell cultures,, in: M.G. Velarde (Ed.), Non-equilibrium Cooperative Phenomena in Physics and Related Fields, Plenum, New York, 1984, p. 241.
[26] A.V. Kuznetsov, The onset of bioconvection in a suspension of gyrotactic microorganisms in a fluid layer of finite depth heated from below, Int. Commun. Heat Mass Tran. 32 (5) (2005) 574–582.
[27] N.S. Khan, T. Gul, M.A. Khan, E. Bonyah, S. Islam, Mixed convection in gravity-driven thin film non-Newtonian nanofluids flow with gyrotactic microorganisms, Res. Phys. 7 (2017) 4033–4049.
[28] S. Zuhra, N.S. Khan, S. Islam, Magnetohydrodynamic second grade nanofluid flow containing nanoparticles and gyrotactic microorganism, Comput. Appl. Math. 37 (2018) 6332–6358, https://doi.org/10.1007/s40314-018-0683-6.
[29] A. Mahdy, Gyrotactic microorganisms mixed convection nanofluid flow along an isothermal vertical wedge in porous media, Int. J. Aero. Mech. Eng. 11 (4) (2017).
[30] R. Sivaraj, I. L. Animasaun, A. S. Olabiyi, S. Saleem, and N. Sandeep, "Gyrotactic Microorganisms and Thermoelectric Effects on the Dynamics of 29 Nm CuO-Water Nanofluid over an Upper Horizontal Surface of Paraboloid of Revolution," Multidiscipline Modeling in Materials and Structures..
[31] M. Khan, T. Salahuddin, M.Y. Malik, M.S. Alqarni, A.M. Alqahtani, Numerical modeling and analysis of bioconvection on MHD flow due to an upper paraboloid surface of revolution, Phys. Stat. Mech. Appl. 553 (2020) 124231, https://doi.org/10.1016/j.physa.2020.124231.
[32] A.M. Rashad, A.J. Chamkhab, B. Mallikarjunac, M.M.M. Abdoua, Mixed bioconvection flow of a nanofluid containing gyrotactic microorganisms past a vertical slender cylinder, Front. Heat Mass Transf. 10 (21) (2018).
[33] L. U. Dianchen, M. Ramzan, N. Ullah, J. D. Chung, and U. Farooq, "A numerical treatment of radiative nanofluid 3D flow containing gyrotactic microorganism with anisotropic slip, binary chemical reaction and activation energy," Sci. Rep. 7, 17008..
[34] Y. Li, H. Waqas, M. Imran, U. Farooq, F. Mallawi, I. Tlili, A numerical exploration of modified second-grade nanofluid with motile microorganisms, thermal radiation, and Wu's slip, Symmetry 12 (3) (2020) 393.
[35] C.S.K. Raju, M.M. Hoque, T. Sivasankar, Radiative flow of Casson fluid over a moving wedge filled with gyrotactic microorganisms, Adv. Powder Technol. 28 (2) (2017) 575–583.
[36] L. Wu, A slip model for rarefied gas flows at arbitrary Knudsen number, Appl. Phys. Lett. 93 (25) (2008) 253103.
[37] T. Fang, S. Yao, J. Zhang, A. Aziz, Viscous flow over a shrinking sheet with a second order slip flow model, Commun. Nonlinear Sci. Numer. Simulat. 15 (7) (2010) 1831–1842.
[38] T. Fang, A. Aziz, Viscous flow with second-order slip velocity over a stretching sheet, Z. Naturforsch. 65 (12) (2010) 1087–1092.
[39] M.M. Nandeppanavar, K. Vajravelu, M.S. Abel, M. Siddalingappa, Second order slip flow and heat transfer over a stretching sheet with non-linear Navier boundary condition, Int. J. Therm. Sci. 58 (2012) 143–150.
[40] K.R. Rajagopal, A.S. Gupta, T.Y. Na, A note on the Falkner-Skan flows of a non-Newtonian fluid, Int. J. Non Lin. Mech. 18 (4) (1983) 313–320.
[41] B.L. Kuo, Application of the differential transformation method to the solutions of Falkner-Skan wedge flow, Acta Mech. 164 (2–3) (2003) 161–174.
[42] A. Ishak, R. Nazar, I. Pop, Falkner-Skan equation for flow past a moving wedge with suction or injection, J. Appl. Math. Comput. 25 (2007) 67–83, https://doi.org/10.1007/BF02832339.
[43] S. M. Atif, S. Hussain, M. Sagheer Heat and mass transfer analysis of time-dependent tangent hyperbolic nanofluid flow past a wedge. Phys. Lett.. DOI: https://doi.org/10.1016/j.physleta.2019.01.003..
[44] T. Salahuddin, I. Khan, M.Y. Malik, M. Khan, A. Hussain, M. Awais, Internal friction between fluid particles of MHD tangent hyperbolic fluid with heat generation: using coefficients improved by Cash and Karp, Eur. Phys. J. Plus 132 (5) (2017) 205–214.